PROCEEDINGS, Thirty-Fifth Workshop on Geothermal Reservoir Engineering
Stanford University, Stanford, California, February 1-3, 2010
SGP-TR-188

APPLICATION OF SELF-POTENTIAL MEASUREMENTS TO GEOTHERMAL RESERVOIR ENGINEERING: CHARACTERIZATION OF FRACTURED RESERVOIRS

Tsuneo Ishido[1], Yuji Nishi[2] and John W. Pritchett[3]

[1, 2]Geological Survey of Japan, AIST
Central 7
Tsukuba, 305-8567, Japan
[1]e-mail: ishido-t@aist.go.jp
[2]e-mail: y.nishi@aist.go.jp

[3]Science Applications International Corp.
10260 Campus Point Drive
San Diego, CA92121
e-mail: John.W.Pritchett@saic.com

ABSTRACT

An "EKP-postprocessor" computational tool was developed several years ago to calculate space/time distributions of electrokinetic potentials resulting from histories of underground conditions (pressure, temperature, liquid-phase saturation, concentration of dissolved species, etc.) computed by unsteady multi-dimensional geothermal reservoir simulations (Ishido and Pritchett, 1996). Since that time, the postprocessor has been applied to various geothermal reservoir engineering problems. The results of numerical simulation calculations to study the possibility of characterizing fractured reservoirs using a combination of pressure and self-potential transient data are presented in this paper.

INTRODUCTION

Mass and heat transport through fractured rock are often modeled numerically using the "MINC" double-porosity representation (Pruess and Narasimhan, 1982). In such reservoir descriptions, the global mass exchange between adjacent macroscopic computational grid blocks takes place mainly through the "fracture zone". Inter-block flow through the "matrix region" is relatively unimportant and is usually neglected in most MINC treatments. But this approximation is inappropriate when calculating the global "drag current" caused by electric charges moving with the flowing fluid due to electrokinetic coupling. Since the magnitude of the drag current density is proportional not to the permeability but to the porosity of the medium, the contribution of the drag current through the matrix region to the total global current between adjacent macroscopic grid blocks is not negligible, and in fact usually predominates under steady-state conditions (Ishido and Pritchett, 2003).

Ishido and Pritchett (2003) extended the so-called EKP-postprocessor (Ishido and Pritchett, 1996) to apply it to fractured reservoirs represented by MINC double-porosity media. They carried out pressure-transient simulations and calculated associated "self-potential transients" by using the extended EKP-postprocessor, and showed that the above property of the drag current brings about much more pronounced differences in the self-potential transients between competing "fractured/ MINC" and "porous-medium" descriptions of the same reservoir than is the case for pressure transients.

Ishido and Pritchett (2003) discussed, however, only the "free-field" SP signals. For comparisons with actual field measurements, we need to take into account the "near-field" effects due to the presence of a borehole, which might short-circuit the fracture and matrix regions both in pressure and electric potential (Pritchett et al., 2006). In the present study we constructed a reservoir model which treats a borehole and individual fractures explicitly and carried out numerical simulation of pressure transients. Then the EKP-postprocessor was applied to calculate observable SP transients either in an open hole or in a cased well.

SP TRANSIENTS IN "MINC" MEDIA

Electrokinetic Coupling

The flow of a fluid through a porous medium will generate an electrical potential gradient (called the electrokinetic or streaming potential) along the flow path by the interaction of the moving pore fluid with

the electrical double layer at the pore surface. This process is known as electrokinetic coupling. The general relations between the electric current density **I** and fluid volume flux **J**, and the electric potential gradient $\nabla\phi$ and pore pressure gradient ($\nabla P - \rho \mathbf{g}$) forces are

$$\mathbf{I} = - L_{ee} \nabla\phi - L_{ev} (\nabla P - \rho \mathbf{g}) \quad (1)$$

$$\mathbf{J} = - L_{ve} \nabla\phi - L_{vv} (\nabla P - \rho \mathbf{g}) \quad (2)$$

where the L_{ij} are phenomenological coefficients (e.g. Ishido and Mizutani, 1981). The first term on the right-hand side in (1) represents Ohm's law and the second term in (2) represents Darcy's law. The cross-coupling terms (with the L_{ev} and L_{ve} coefficients) represent the electrokinetic effect; $L_{ev} = L_{ve}$ according to Onsagar's reciprocal relations.

Based upon a capillary model, the above coefficients may be written as follows (Ishido and Mizutani, 1981):

$$L_{ev} = -\eta \varepsilon \zeta R_{ev} G/\tau \mu \quad (3)$$

$$L_{ee} = \eta(\sigma + m^{-1}\Sigma_s)/ \tau \quad (4)$$

where:

η = porosity,
ε = liquid-phase dielectric permittivity,
ζ = zeta-potential,
R_{ev} = "electrical relative permeability" for two-phase flow,
G = correction factor which becomes less than unity only if the hydraulic radius is comparable to the thickness of the electrical double layer,
τ = square of tortuosity ($\tau = t^2$),
μ = liquid-phase viscosity,
σ = electrical conductivity of pore fluid,
m = hydraulic radius of pores and/or cracks,
Σ_s = surface conductance.

Equation (1) describes the total current density, composed of a drag (convection) current density $\mathbf{I}_{drag}$ caused by charges moved by fluid flow, and a conduction current density $\mathbf{I}_{cond}$ caused by electric conduction; hence,

$$\mathbf{I} = \mathbf{I}_{cond} + \mathbf{I}_{drag} \quad (5)$$

where

$$\mathbf{I}_{cond} = -L_{ee} \nabla\phi$$

$$\mathbf{I}_{drag} = -L_{ev} (\nabla P - \rho \mathbf{g})$$

In the absence of external current sources, $\nabla \cdot \mathbf{I} = 0$, so from (5):

$$\nabla \cdot \mathbf{I}_{cond} = - \nabla \cdot \mathbf{I}_{drag} \quad (6)$$

Equation (6) represents sources of conduction current that are required for the appearance of electrical potential.

In a homogeneous region, (6) can be written as:

$$\nabla^2\phi = C \nabla^2(P - \rho g z) \quad (7)$$

where C is called the streaming potential coefficient:

$$C = -L_{ev}/ L_{ee} = \varepsilon \zeta / (\sigma + m^{-1}\Sigma_s)\mu \quad (8)$$

If the pore pressure change occurs within a finite homogeneous volume, the following relation between changes in ϕ (streaming potential) and ($P - \rho g z$) (pressure) prevails:

$$\Delta\phi = C \Delta(P - \rho g z) \quad (9)$$

EKP-Postprocessor

The cross-coupling term in (2) may be safely neglected for typical geologic situations, and Darcy's law alone may be used to model the hydraulic problem; it is not necessary to solve (1) and (2) simultaneously. A "postprocessor" may then be used to calculate the drag current ($\mathbf{I}_{drag}$) from the results of an unsteady thermohydraulic reservoir simulation.

The "EKP-postprocessor" (Ishido and Pritchett, 1996; see also Ishido and Pritchett, 1999) simulates electric potentials caused by subsurface fluid flow by a two-step process. First, it calculates the distribution of L_{ev}, L_{ee} and $\mathbf{I}_{drag}$ from the reservoir-simulation results using the same spatial grid used for the reservoir simulation calculation (called the RSV-grid hereafter). Next, the postprocessor calculates the electric potential (ϕ) distribution by solving the above Poisson equation (6) within a finite-difference grid that is usually much greater in spatial extent than the RSV-grid (hereafter called the SP-grid).

Within that portion of the SP-grid overlapped by the RSV-grid, the distribution of electrical conductivity is obtained directly from RSV-grid values. Elsewhere within the SP-grid, the electrical conductivity distribution is user-specified and time-invariant. Ordinarily, boundary conditions on the potential are: zero normal gradients (Neumann condition) on the ground surface (upper surface) and zero potential (Dirichlet condition) along the bottom and vertical sides of the SP-grid. Equation (6) is solved numerically using a Gauss-Seidel iteration procedure incorporating intermittent automatic optimization of the overrelaxation factor.

The EKP-postprocessor was originally developed as one of the mathematical postprocessors for the "STAR" code (e.g., Pritchett, 1995). The reservoir-simulation results required for postprocessor calculations are stored on the so-called "*GEO*" output file.

Model for Drag Current in MINC Media

The model which Ishido and Pritchett (2003) adopted to calculate the drag current density in "MINC" media (Pruess and Narasimhan, 1982) amounts to the following:

$$\mathbf{I_{total}} = \mathbf{I_f} + \mathbf{I_m} \quad (10)$$

with:

$$\mathbf{I_f} = [\varepsilon\zeta\eta R_{ev} G(\nabla P - \rho\mathbf{g})/\tau\,\mu]_f \times \psi \quad (11)$$

$$\mathbf{I_m} = [\varepsilon\zeta\eta R_{ev} G(\nabla P - \rho\mathbf{g})/\tau\,\mu]_m \times (1 - \psi) \quad (12)$$

where:

$\mathbf{I_{total}}$ = total drag current density vector,
$\mathbf{I_f}$ = drag current density due to fracture zone effects,
$\mathbf{I_m}$ = drag current density due to matrix region effects,
ψ = fracture zone volume / total volume,

and where subscript "f" denotes conditions in the fracture zone, and subscript "m" denotes "averaged" conditions in the matrix region.

The EKP postprocessor computes the "fracture zone" drag current based on the liquid-phase mass flux in the fracture zone ($\mathbf{M_f}$) using Darcy's law:

$$\mathbf{M_f} = [Rk\rho\,(\rho\mathbf{g} - \nabla P)/\mu]_f \quad (13)$$

so that:

$$\mathbf{I_f} = -\psi\,[\mathbf{M}\varepsilon\zeta\eta\,(R_{ev}/R)G/\,(\rho\tau k)]_f \quad (14)$$

where "R" is liquid-phase relative permeability and the quantities within the brackets refer to conditions in the fracture zone. $\mathbf{M_f}$ is obtained directly from STAR's *"GEO"* output file. Although the average mass flux in the matrix region ($\mathbf{M_m}$) can be assumed to be negligible compared to $\mathbf{M_f}$, i.e. $|\mathbf{M_f}| >> |\mathbf{M_m}|$, $k_f >> k_m$ as well, so that the quantities $(\mathbf{M}/k)_f$ and $(\mathbf{M}/k)_m$ can be comparable in magnitude.

In the present model, the value of $\mathbf{I_{total}}$ is assumed to be expressable as:

$$\mathbf{I_{total}} = \mathbf{I_f}\,[1 + (\mathbf{I_m}/\mathbf{I_f})] \approx \mathbf{I_f}\,(1 + F) \quad (15)$$

where $\mathbf{I_f}$ is calculated using (14), and where the scalar factor F is given by:

$$F = B \times V \times D \quad (16)$$

with:

$$B = [(R_{ev}/S)_m/(R_{ev}/S)_f] \times [(\varepsilon\zeta G/\tau\mu)_m/(\varepsilon\zeta G/\tau\mu)_f] \quad (17)$$

$$V = (1 - \psi)\,\eta_m\,S_m / \psi\,\eta_f\,S_f \quad (18)$$

$$D = [(\nabla P - \rho\mathbf{g})_m / (\nabla P - \rho\mathbf{g})_f] \quad (19)$$

In the above equations, "S" denotes liquid-phase saturation, in either the "fracture zone" (S_f) or the "matrix region" (S_m). Note that "B" is typically of order unity or less (see Ishido and Matsushima, 2007 for laboratory measurements of the coupling coefficient of intact rock sample), "V" is simply the ratio of the liquid volume in the matrix region to that in the fracture zone, and "D" (the ratio of pressure gradients) will usually lie between zero and unity. The factor B is approximated as a user-prescribed unchanging function of position ("formation type") in the present version of the postprocessor. Note that, if B = 1 everywhere, under steady-state single-phase liquid conditions the drag current density calculated in this way is identical to that for an equivalent porous medium.

To calculate the grid-block-face drag current density within the RSV-grid, ψ, η, τ, k, G and ζ in (14) and B, V in (16) are computed at grid block interfaces using harmonic means. Other interface quantities in (14) are treated using a second-order upstream weighting scheme. The EKP-postprocessor solves (6) by inserting (10) into the right hand side of (6) and obtains "averaged" electric potential in each grid block represented by a MINC-medium.

Pressure and SP Transients in MINC Media

Ishido and Pritchett (2003) performed a pressure-transient simulation for a two-dimensional axi-symmetric horizontal reservoir model. The formation is represented by a "MINC" double- porosity medium with the following properties:

global permeability: $k = 10^{-14}$ m^2,
fracture zone volume fraction: $\psi = 0.1$,
fracture zone porosity: $\eta_f = 0.1$,
matrix region porosity: $\eta_m = 0.1$,
matrix region permeability: $k_m = 10^{-17}$ m^2,
fracture spacing: $\lambda = 10$ m.

The time required ($\tau_{pe} = \eta_m\,\mu\,C\lambda^2/10\,k_m$) for pressure equilibration between the fracture and matrix regions is ~10^4 sec. The initial thermodynamic state is uniform (temperature = 200°C and pressure = 10 MPa).

For the corresponding SP calculations, the reservoir fluid's NaCl concentration is assumed to be 0.002 mol/L, and the formation conductivity L_{ee} is constant at 0.003 S/m. The tortuosities are assumed to be 1 (τ =1) both for the fracture and matrix regions.

Figure 1 shows semi-log plots of changes in pressure and in SP due to continuous injection at 0.5 tons per hour per meter of reservoir thickness. The pressure transient at a point near the injection well shows behavior typical of a double-porosity medium: the late-time slope develops after the time required for pressure equilibrium within the matrix region τ_{pe} has elapsed. The SP transient also exhibits three segments.

The drag current contribution through the matrix region is small at early times, so the slope is smaller than that at late times, by the factor ψ (= 0.1). At intermediate times, SP changes rapidly with increasing involvement of matrix region. The time τ_{pe} can be clearly identified at the intersection of the intermediate-time and late-time semi-log straight lines.

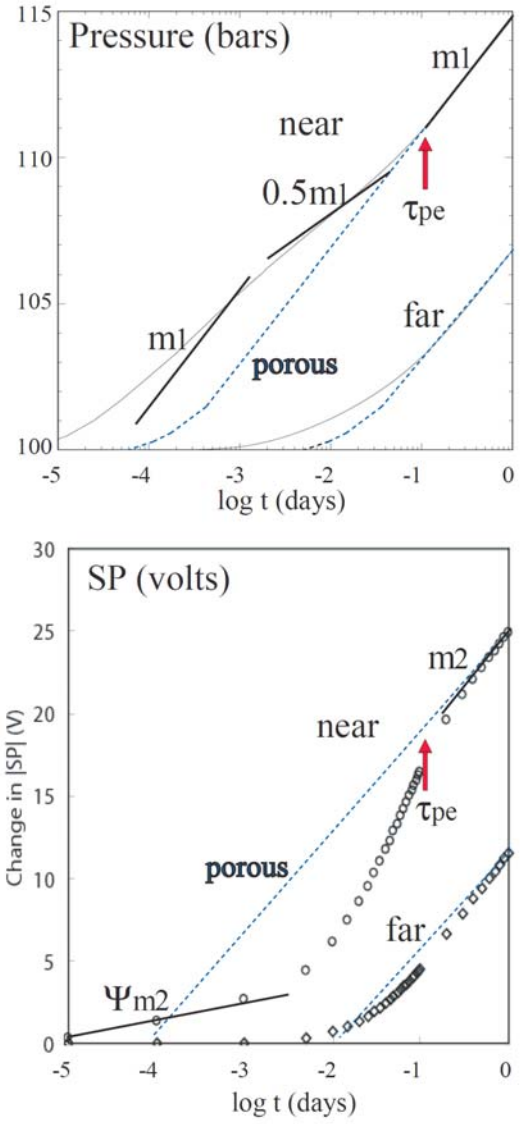

Figure 1: Changes in pressure and SP during injection test for fractured medium with fracture spacing of 10 m (after Ishido and Pritchett, 2003). The results for the equivalent porous medium are shown by broken curves. Labels "near" and "far" indicate that the observation point is ~5 m and ~50 m away from the injection well, respectively. Note that the magnitudes of SP changes shown here are quite large: a few tens of volts. This is brought about by a combination of assumed values of pertinent parameters. If the porosity and electrical conductivity are assumed to be 0.01 and 0.03 S/m, respectively instead of 0.1 and 0.003 S/m, respectively in the calculation, the magnitudes will be reduced to a few hundreds of milli-volts.

Figure 2 shows the ratio of SP changes to pressure changes for the results shown in Figure 1. In the case of the equivalent porous medium, relationship (9) is satisfied for the entire period, resulting in an almost constant ratio. In this plot, the differences between double-porosity and equivalent porous medium behavior is much more apparent and the time τ_{pe} is more evident than in a plot of SP change itself (Figure 1). The change-ratio plot has the additional advantage that, in real situations, pressure transient data suffer from fluctuations in the sandface flow-rate, so it is often difficult to discern the three segments such as those shown in Figure 1. By contrast, the ratio of SP-change to pressure-change is insensitive to flow-rate fluctuations, so a combination of pressure and SP measurements is expected to provide a more robust and reliable technique for fractured reservoir characterization.

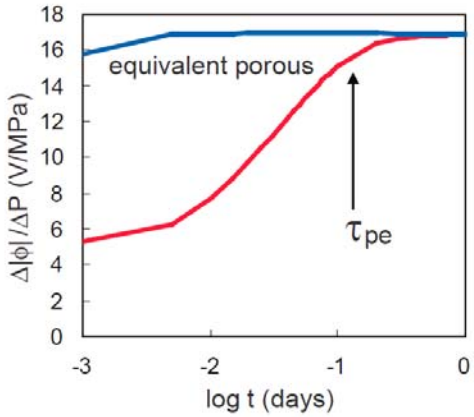

Figure 2: Plot of the ratio of SP change to pressure change for the "double-porosity" and "equivalent porous medium" results shown in Fig. 1.

NEAR-FIELD EFFECTS

In the calculations described in the previous section, Ishido and Pritchett (2003) did not consider the "near-field" effects around a borehole. In the present study, we constructed a reservoir model to treat a borehole and individual fractures explicitly instead of using the MINC double-porosity representation. The model is axi-symmetric, eight meters thick, and of 1 km horizontal extent (radius). Five equally-spaced horizontal fractures intersect the borehole located along the axis of symmetry. We adopted sufficiently fine block spacing near the borehole (radius of 0.075 meter) to represent the well casing. Fine block spacing was also used for the host rock (matrix) region close to the fracture zone so as to resolve the high electrical potential gradients there.

The formation properties are:

fracture zone permeability: $k = 10^{-12}$ m^2,
fracture zone thickness = 0.01 m,
fracture zone porosity: $\eta_f = 0.5$,
host rock porosity: $\eta_m = 0.01$,
host rock permeability: $k_m = 10^{-18}$ m^2,
fracture spacing: $\lambda = 1$ m.

The time required (τ_{pe}) for pressure equilibration between the fracture and matrix regions is ~500 sec. The initial thermodynamic state is uniform (temperature = 45°C and pressure = 10 MPa).

For the corresponding SP calculations, the reservoir fluid's NaCl concentration is assumed to be 0.005 mol/L, and the streaming potential coefficient is uniform throughout the fracture and host rock regions.

Open Hole SP Transients

Figure 3 shows the electrical potential distribution in the central region (r < 15 meters) at early and intermediate times caused by fluid production from the borehole with a constant pressure drawdown of 1 MPa. The SP disturbance is confined to the fracture zones at early times and later expands into the matrix region as the pressure disturbance diffuses from the fractures into the matrix region. Since the streaming potential coefficient is assumed to be homogeneous, SP change corresponds exactly to pressure change as described by (9) in this case.

In the "open hole" cases, the SP change that would be measured by electrode(s) installed within the borehole (Figure 4) is calculated, and then the ratio of SP change to pressure change is plotted as a function of time (Figure 5). As Figure 5 shows, the (dark blue) "open" ratio is almost constant with time, which is similar to the "equivalent porous medium" behavior shown in Figure 2, and does not exhibit any characteristic fractured reservoir behavior.

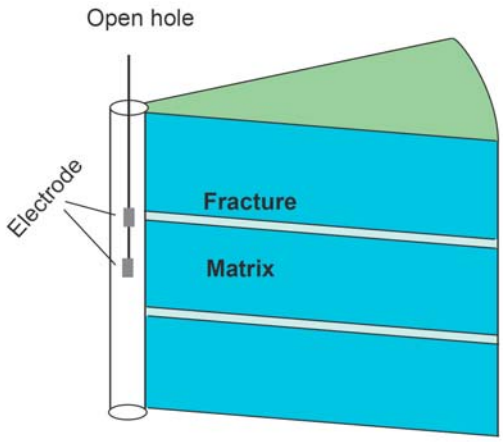

Figure 4: SP sensors deployed on a wireline in open hole interval.

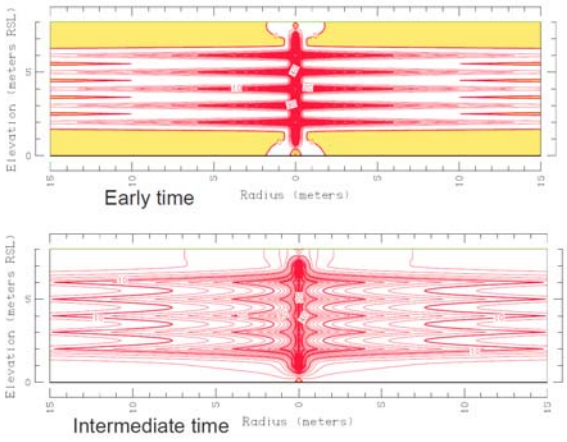

Figure 3: Vertical section of equi-potential surfaces at early (~43 sec) and intermediate (~430 sec) times for "open hole" case.

But if a skin zone in which the streaming potential coefficient is much smaller than that of the outer matrix region is present, the typical double-porosity behavior appears in the plot (blue "open (skin)" curves in Figure 5). Although the SP change magnitude is independent of the location of the electrode for the case without a skin zone, the SP change is slightly smaller at the electrode located at the matrix region for the case with skin zone as shown by the broken line in Figure 5.

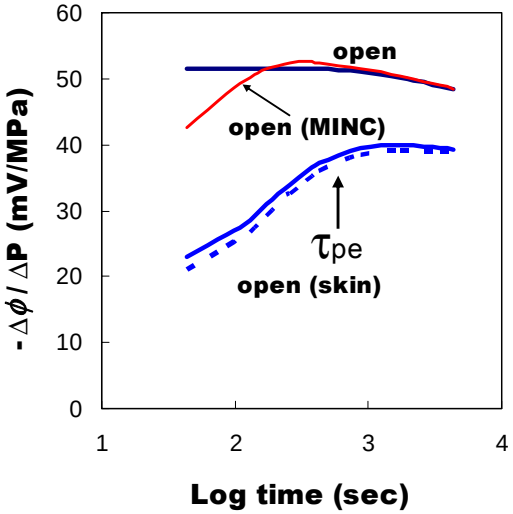

Figure 5: The ratio of SP change to pressure change as a function of time for "open hole" cases. The ratio's for the case with a skin zone are labeled "open (skin)", and the ratio calculated for MINC representation is labeled "open (MINC)".

Figure 6 illustrates the spatial distribution of "microscopic" potential, which is the streaming potential coefficient multiplied by local pressure change, in the fracture and matrix regions around an open hole. Along the wall of the open hole, the local pressures in both the fracture and matrix regions are equal to the borehole pressure, so the microscopic potentials in the both regions converge as the borehole is approached. This is the reason why the SP change is in proportion to the pressure change within the borehole in the "open" case. However, in the "open (skin)" case, substantial drag current is not induced in the matrix region while a large pressure gradient remains within the skin zone. So, SP change within the borehole is brought about solely by the drag current induced in the fracture zone, resulting in smaller SP change magnitude at early times.

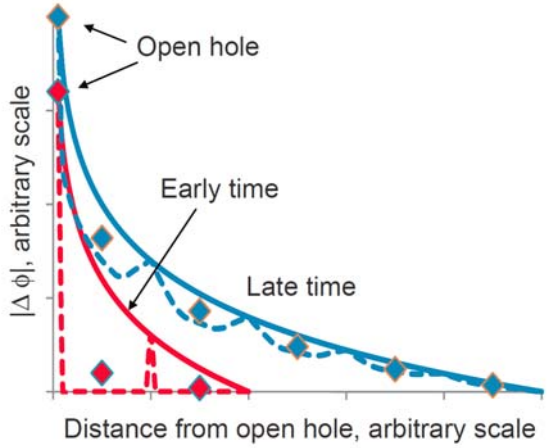

Figure 6: Schematic diagram showing the distribution of "microscopic" potential in the fracture (solid lines) and matrix (broken lines) regions, which is equal to change in local pressure multiplied by the streaming potential coefficient C (here homogeneous C is assumed for simplicity). "Macroscopic" potential (♦) calculated for MINC-medium blocks corresponds to an averaged potential over the fracture and matrix regions.

In Figure 5, also shown (in red) is the result for a case in which the reservoir is represented by "equivalent" MINC double-porosity medium. In this "open (MINC)" case, the SP/pressure change ratio exhibits similar behavior as that of "open" case. This is because the present scheme used by the EKP-postprocessor to calculate SP in a MINC medium gives an "averaged" potential over the fracture and matrix regions.

Observations in Cased Wells

Next we consider cased wells, in which the hydraulic communication between the borehole and the formation is restricted to the fracture region. Direct hydraulic contact between the borehole and matrix region is prevented by solid casing and cementing.

If the casing pipe consists of a material that is not electrically conductive, SP will be measured using small electrodes installed outside the casing (Figure 7). Electrode response depends in this case on

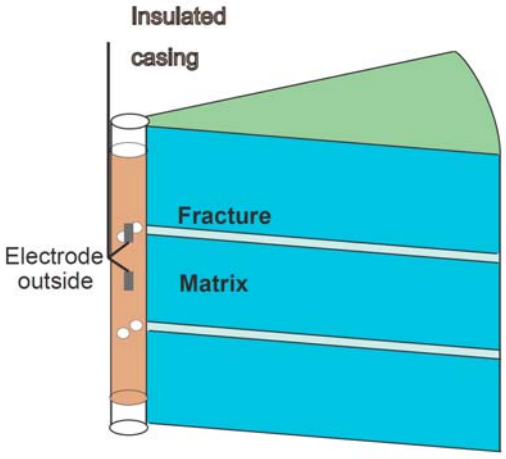

Figure 7:Electrodes are attached on the outside of the insulated casing, and cemented in place. The casing is perforated only at fracture zone.

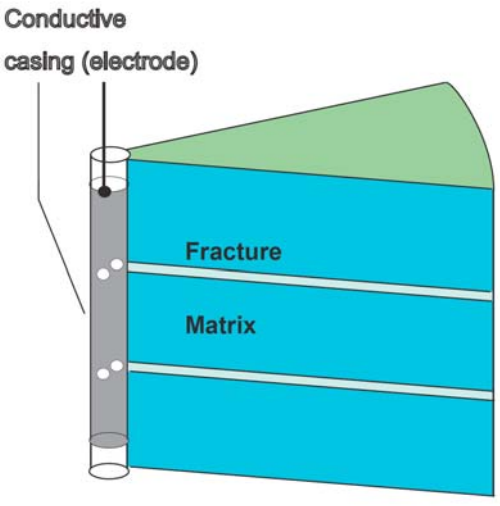

Figure 8: Electrically conductive casing, which is cemented in place and perforated only at fracture zone, is used as electrode.

whether the electrode is situated in the fracture zone or in the matrix region. The normalized SP change is nearly constant near the fractures, but in the matrix region it is small at early times and rapidly increases as time approaches τ_{pe}, reflecting the pressure change in the matrix region (green curves in Figure 9).

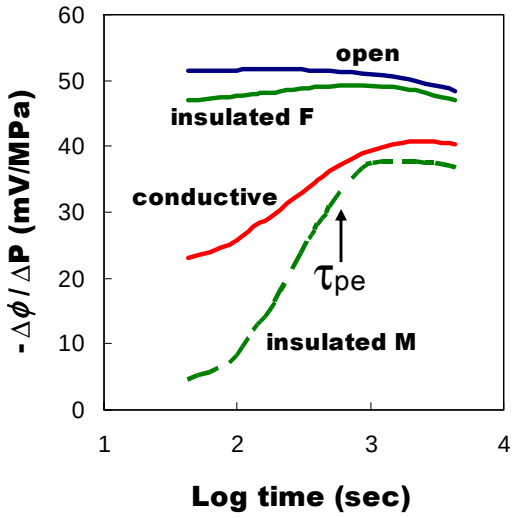

Figure 9: The ratio of SP change to pressure change as a function of time for "cased well" cases. (The ratio labeled "open" is the same as that shown in Fig. 5.)

If the casing material is conductive as in the more typical case of metallic casing pipe (Figure 8), the potential of the casing itself is measured. The normalized SP change is indicated by the red curve labeled "conductive" in Figure 9, and represents an averaged behavior of the matrix and fractured regions.

Observations at the Kamaishi Mine

The Kamaishi Mine is located in Iwate prefecture in Japan. We carried out measurements in two open holes (KF-1 and KF-3) which are drilled nearly horizontally from the wall of one of the tunnels into the surrounding granodiorite body. Both wells maintain stable pressures of about five bars under shut-in conditions, so that flow tests may be carried out by simply opening and closing the wellhead valves. After preliminary experiments in 2005 and 2006 (Nishi et al., 2006), we installed twelve silver-silver chloride electrodes in each of the two wells in 2007 (Nishi et al., 2008).

The ratio of SP change to pressure change is shown in Figure 10. We observed (very reproducible) behavior which depended upon whether or not the electrode was located adjacent to a fracture. This ratio is almost constant after 100 seconds for electrodes located in the relatively impermeable country rock zone, but exhibits double porosity behavior near the fractures, which can be explained by the "open hole with skin" model behavior discussed in the preceding section.

This double porosity behavior is particularly evident in the results from the KF-1 electrodes. Based on the observed τ_{pe} value (~1000 seconds) and the matrix rock permeability (several microdarcies) deduced by testing core samples, we may estimate the fracture spacing to be a few meters. This is in good agreement with the value inferred from detailed geological observations.

The ratio of SP disturbance to pressure disturbance corresponds to the streaming potential coefficient C, and is about -10 mV/MPa for the non-fractured country rock zone (this value is in the range of C measured for an intact granite sample in dilute solutions by Ishido and Matsushima, 2007). As for the fracture zone, the final asymptotic value is also about -10 mV/MPa. This suggests that the contribution of drag current through the matrix region dominates under steady-state conditions.

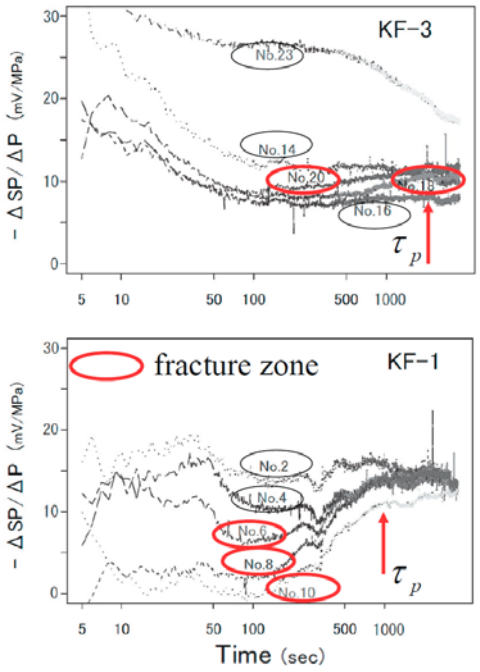

Figure 10: The ratio of SP change to pressure change as a function of time for 2007 observations in open holes KF-1 and KF-3 at the Kamaishi Mine (after Nishi et al., 2008). Electrodes located adjacent to a fracture and in the country rock zone are indicated by red and black ellipses, respectively.

CONCLUDING REMARKS

- The present calculations show that the ΔSP/ΔP observation is useful for characterizing fractured reservoirs.
- To detect microscopic ΔSP/ΔP, an electrode array installed outside the insulated casing is desirable. Such observations were recently reported from an oil field by Chen et al. (2006).
- To detect macroscopic ΔSP/ΔP such as predicted by Ishido and Pritchett (2003), the conductive casing itself (with electrical continuity extending over a distance longer than the typical fracture spacing) can be used as an electrode.
- In open holes, the appearance of double porosity behavior depends on whether or not a skin zone is present.
- Double porosity behavior was observed in the open hole experiments at the Kamaishi mine for electrodes located adjacent to fractures.
- It may be that skin zones will be found in most open hole completions, so measurements of this type in open holes are likely to be useful.

REFERENCES

Chen, M.-Y., Raghuraman, B., Bryant, I. and Supp, M. (2006), "Streaming Potential Applications in Oil Fields," paper *SPE* 102106 presented at *the 2006 Annual Technical Conference and Exhibition*, San Antonio, 24-27 Sep. 2006.

Ishido, T. and Mizutani, H. (1981), "Experimental and Theoretical Basis of Electrokinetic Phenomena in Rock-Water Systems and its Applications to Geophysics," *Journal of Geophysical Research*, **86**, 1763-1775.

Ishido, T., and Pritchett, J.W. (1996), "Numerical Simulation of Electrokinetic Potentials Associated with Subsurface Fluid Flow," *Proc. 21st Stanford Workshop on Geothermal Reservoir Engineering*, 143-149.

Ishido, T., and Pritchett, J.W. (1999), "Numerical Simulation of Electrokinetic Potentials Associated with Subsurface Fluid Flow," *Journal of Geophysical Research*, **104**, 15,247-15,259.

Ishido, T. and Pritchett, J.W. (2003), "Characterization of Fractured Reservoirs Using Continuous Self-Potential Measurements," *Proc. 28th Stanford Workshop on Geothermal Reservoir Engineering*, 158-165.

Ishido, T. and Matsushima, N. (2007), "Streaming Potential Measured for an Intact Granite Sample at Temperatures to 200°C," *Proc. 32nd Stanford Workshop on Geothermal Reservoir Engineering* (CD-ROM).

Nishi, Y., Ishido, T. and Negi, T. (2006), "Field Experiments to Characterize Hydrological Properties of Fractured Rock Using Continuous Borehole Self-Potential Measurement," *Transactions Geothermal Resources Council*, **30** (CD-ROM).

Nishi, Y., Ishido, T. and Negi, T. (2008), "Continuous Borehole Self-Potential Measurement – A New Approach to Characterize Hydrological Properties of Fractured Rock," *Butsuri-Tansa*, **61**, 285-299.

Pritchett, J.W. (1995), "STAR: A Geothermal Reservoir Simulation System," *Proc. World Geothermal Congress*, 2959-2963, IGA, Florence.

Pritchett, J.W., Garg, S.K., Ishido, T., Matsushima, N. and Livesay, B.J. (2006), "Evaluating Permeability Enhancement Using Electrical Techniques," *Final Technical Report for Year 2*, DOE Award Number DF-FG36-04GO14291.

Pruess, K. and Narasimhan, T.N. (1982), "A Practical Method for Modeling Fluid and Heat Flow in Fractured Porous Media," presented at *the Reservoir Simulation Symposium of the Society of Petroleum Engineers*, New Orleans, Jan. 31 - Feb. 3. (Also see *SPE Journal*, Feb. 1985, pp.14-26).